Research Article

Mashael A. Aljohani, Arshad Khan*, Wafa F. Alfwzan, Humaira Yasmin, Zehba Raizah, Khadijah M. Abualnaja, and Emad E. Mahmoud

Entropy optimization for chemically reactive magnetized unsteady thin film hybrid nanofluid flow on inclined surface subject to nonlinear mixed convection and variable temperature

https://doi.org/10.1515/phys-2025-0175
received January 18, 2025; accepted June 09, 2025

Abstract: This study aims to investigate thin film flow with the effects of a magnetic field in association with Cu and CuO nanoparticles past an inclined plate. The second law of thermodynamics is used to optimize the production of entropy and to reduce the fluid's friction. The leading equations have been solved through the homotopy analysis method in dimensionless form. It is observed that fluid motion is slowed down as the thickness factor, volumetric fraction of nanoparticles, and unsteadiness parameter increase, while it intensifies with higher values of mass and thermal Grashof numbers. The thermal distribution has augmented with an upsurge in volumetric fraction, magnetic factor, Eckert number, and unsteadiness factor. Bejan number as well as the rate of entropy production are opposed by Brinkman number and are supported by growth in magnetic factor. For nanoparticle volume fractions ranging from 0.01 to 0.03, the Nusselt number shows significant improvement, particularly for hybrid nanoparticles, where it increases from 4.3207 to 6.6983%, demonstrating their superiority over traditional nanoparticles. Validation of work has been ensured through comparative analysis between current results and published works.

Keywords: thin film flow, hybrid nanofluid, electromagnetic field, nonlinear mixed convection, heat and mass transportation, homotopy analysis method

1 Introduction

Thin film flow describes the movement of a fluid layer whose thickness is much smaller. Thin film flows involve the motion of liquid or fluid films with small thickness compared to their lateral dimensions. It has many applications in mechanical engineering as well as manufacturing processes like coating of glass, fluidization of reactor, coating of wire and fiber, *etc.* The concept of thin film over the starched surface has derived by Wang [1]. Qasim *et al.*'s [2] investigation revealed that thin liquid films exhibit the best transfer of mass and heat compared to thicker liquids. This characteristic makes them more suitable for applications where minimal heat is required for maintaining the stability of the thin film. Researchers are currently exploring the use of hybrid nanoparticle fluid films as a coating material for glass surfaces, with the aim of developing solar panels. In the near future, car windows are expected to serve as solar panels, providing energy for both cooling and heating purposes. This innovation offers the potential to seamlessly integrate renewable energy generation and effective thermal management into everyday items. The applications of magnetic and electric fields play a vital role in fluid film dynamics, particularly in microfluidic systems, where electric fields are used to manipulate and disintegrate thin films stretched between suspended microscopic droplets. Sun *et al.* [3] numerically analyzed thin liquid film flow on a spinning disk, considering the effects of nonlinear radiations and a thermal

* **Corresponding author: Arshad Khan,** College of Aeronautical Engineering, National University of Sciences and Technology, Sector H-12, Islamabad, 44000, Pakistan, e-mail: arshad8084@gmail.com
Mashael A. Aljohani: Department of Mathematics and Statistics, College of Science, Taibah University, Yanbu, Saudi Arabia
Wafa F. Alfwzan: Department of Mathematical Sciences, College of Science, Princess Nourah bint Abdulrahman University, P.O. Box 84428, Riyadh, 11671, Saudi Arabia
Humaira Yasmin: Department of Basic Sciences, Preparatory Year Deanship, King Faisal University, P.O. Box 400, Al Ahsa, 31982, Saudi Arabia
Zehba Raizah: Department of Mathematics, Faculty of Science, King Khalid University, Abha, 61413, Saudi Arabia
Khadijah M. Abualnaja, Emad E. Mahmoud: Department of Mathematics and Statistics, Collage of Science, Taif University, P.O. Box 11099, Taif, 21944, Saudi Arabia

source. Their study highlights how these thermal factors influence heat transfer and flow behavior on rotating surfaces. Thin film flow over an inclined plate has numerous applications, including paint finishing in stable dispersions, chemical engineering processes, and surface coating technologies. Various factors like electric as well as magnetic factors are applied to stabilize the uniform dispersion of fluid films for enhancement the glassy texture of the final product. The performance of liquid film upon an inclined surface has been discussed by Kapitza *et al.* [4]. Dholey [5] has extended and refined the idea of Kapitza *et al.* [4] by employing a similar geometrical view and has examined the instability of fluid using magnetic and electric effects.

Flow on a stretching sheet describes the fluid motion that occurs when a flat surface is continuously stretched. This phenomenon finds applications in various industrial processes, like polymer processing and coating deposition. Controlling this flow is vital for optimizing manufacturing processes and improving products' quality. Various metallurgical, mechanical, and designing processes, such as paper fabrication and drawing, glass blowing, and assembling of plastic and elastic sheets, exhibit the flows of different fluids upon stretching sheets. The flow upon stretching the surface was first discussed by Crane [6] for investigating different flow characteristics. Sudarmozhi *et al.* [7] discussed the melting thermal effects on fluid flow past an elongating sheet with thermophoresis effects. Rosca and Pop [8] examined the time-based flow of fluid passing a permeable shrinking/stretching curved sheet. Their findings revealed that as the permeability factor increased, the fluid motion declined. Their results suggest that the permeability of the sheet influences the flow characteristics, affecting the rate of fluid motion on the stretching sheet. Abbas *et al.* [9] inspected magnetized radiative fluid flow over a curved expanding sheet and revealed that growth in magnetic factor has augmented the thermal distribution and has weakened the velocity characteristics. Imtiaz *et al.* [10] investigated the magneto-hydrodynamic (MHD) time-dependent fluid flow on a curved extending sheet with the influence of both homogeneous and heterogeneous reactions. Sanni *et al.* [11] examined the viscous fluid flow progression past a curved as well as nonlinear stretched surface. Hayat *et al.* [12] scrutinized numerically the nanofluid flow induced by nonlinear stretching and curved surface associated with mass and thermal convective constraints. Okechi *et al.* [13] debated on viscous fluid flow on a curved and exponentially elongating surface. Further investigations about the concept of stretching sheet flows can be explored in previous studies [14–16].

Nanofluid flow demonstrates the movement of a liquid containing suspended nanoparticles. Nanofluid flow finds applications in heat exchangers, electronics cooling, energy systems, and biomedical engineering, where enhanced thermal conductivity and improved heat transfer properties offer advantages. Hobiny and Abbas [17] discussed dual-phase lag bio-thermal modeling through living tissues affected by laser irradiations. Optimizing nanofluid flow enables advancements in various industries, enhancing performance and efficiency in diverse engineering and scientific applications. Various investigators have conducted different investigations [18–20] for the augmentation of the thermal performance of pure fluid. Dinarvand *et al.* [21] employed copper and alumina nanoparticles in a two-step method to enhance drug delivery through the microcirculatory system over a permeable and stretched sheet. Shojaie Chahregh and Dinarvand [22] discussed blood-based hybrid nanofluid flow through an artery to facilitate drug delivery and blood rotation within the respiratory system. Their study focused on developing a fundamental model to understand the rotational behavior of blood and the distribution of medicines in the respiratory system. Chamkha *et al.* [23] investigated heat and mass transfer using variable temperature and concentration conditions, considering the combined effects of chemical reactions and nanoparticle shape. They found that fluid velocity decreased, while thermal distribution increased with higher nanoparticles' concentration. Khan *et al.* [24] studied heat transfer in bio-convective hybrid nanofluid flow on a heated moving needle and deduced that the Nusselt number has increased with a surge in Eckert number, thermophoresis, and Brownian motion effects. Gul *et al.* [25] examined Marangoni convection in MHD blood-based carbon nanotubes nanofluid flow and noted a reduction in velocity and augmentation in thermal profiles as nanoparticle concentration increased. Kamis *et al.* [26] explored the influence of suction on unsteady hybrid nanofluid film flow over a stretched sheet.

The transfer of mass in various species mostly occurs when there is a variation in the concentration of these species. Due to this concentration gradient, the migration of species from higher to lower concentration zones has been noticed. Such phenomena can be found in the diffusion of nutrients inside tissues, thermal insulation, and the handling of foods. In the past few decades, the transmission of mass subject to chemical reaction has remained an active field of research. Hobiny and Abbas [27] conducted experimental investigations to analyze the thermal responses of cylindrical biological tissues under laser irradiation, providing insights into heat distribution and temperature rise. Their study contributed to understanding laser–tissue interactions, which is vital in medical applications like laser surgery, therapy, and tissue engineering. Marin *et al.* [28] studied

a nonlinear bio-heat model for skin tissues with the impacts of external heat sources. Eid *et al.* [29] explored the Prandtl number using the impact of high-order chemical reactions on the motion of nanofluid and concluded that the magnetic effect has augmented the thermal distribution and skin friction. Dhlamini *et al.* [30] inspected mixed convective and binary chemically reactive flow of nanofluid and revealed that with progress in chemical reaction factor, the concentration of fluid has augmented. Saeed and Abbas [31] examined experimentally the utilization of the finite-element approach for a non-linear bio-heat model for spherical tissues.

This research work develops a mathematical model for hybrid nanofluid flow on an inclined surface. The following points highlight the novelty of this study:

- The work of Qasim *et al.* [2] has been expanded by incorporating inclined and stretching surfaces to investigate the unsteady thin film fluid flow, which has not been discussed yet in the presence of nonlinear mixed convection.
- The inclusion of an inclined surface introduces an additional factor that influences the fluid dynamics and flow behavior.
- Furthermore, the incorporation of stretching surfaces adds another dimension to the analysis, considering the effects of surface deformation on fluid flow.
- Nonlinear mixed convection has been added to the proposed model in mathematical form along with the impacts of a variable magnetic field.
- By incorporating variable temperature and concentration, the research provides valuable insights into the thermal and concentration gradients that affect the fluid flow, particularly in the vicinity of the inclined surface.
- Homotopy analysis method (HAM) has been employed to solve the proposed mathematical model.

2 Formulation of the problem

A thin plate is considered with θ being an angle of inclination of the sheet with the horizontal axis as exhibited in Figure 1. The following assumptions are made:

- The sheet behaves as elongating with velocity $U_w = bx(1-at)^{-0.5}$ with $b(1-at)^{-0.5}$ an operative rate of elasticity that exhibits an enhancing behavior on the domain $0 \le a < 1$ such that $a, b > 0$ and b is the elasticity constant.
- The variable temperature and concentration at surface of elongating sheet are described as $T_s(x,t) = T_0 - T_{\text{ref}}(bx^2/2v)(1-at)^{-\frac{3}{2}}$ and $C_s(x,t) = C_0 - C_{\text{ref}}(bx^2/2v)(1-\gamma t)^{-3/2}$,

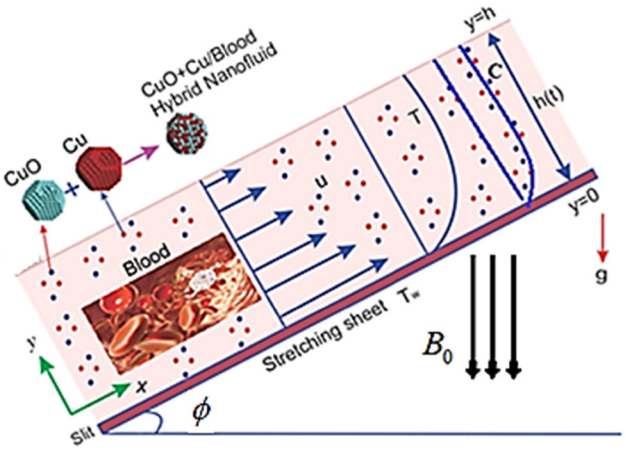

Figure 1: Graphical view of the flow problem.

where T_0, T_{ref} and C_0, C_{ref} are slit and constant reference temperatures and concentrations such that $0 < T_{\text{ref}} < T_0$ and $0 < C_{\text{ref}} < C_0$.

- The term $(bx^2/v(1-at) = xU_w/v)$ describes the local Reynolds number that is based upon U_w (surface velocity).
- Variable magnetic effects with strength $B_0(x,t) = B_0(1-at)^{-0.5}$ have been considered in the transverse direction of flow.
- The thickness of the film is $h(t)$ that is positioned on the inclined sheet.
- The temperature of sheet varies from T_0 at the slit which is in direct proportion to x^2, where the amount of temperature drops with growth in time.

With the help of the above assumptions, the leading equations are

$$\frac{\partial u}{\partial x} + \frac{\partial v}{\partial y} = 0, \tag{1}$$

$$\begin{aligned}\frac{\partial u}{\partial t} + u\frac{\partial u}{\partial x} + v\frac{\partial u}{\partial y} &= \upsilon_{\text{hnf}}\left(\frac{\partial^2 u}{\partial y^2} + \frac{\partial^2 u}{\partial x^2}\right) - \frac{\sigma_{\text{hnf}}u}{\rho_{\text{hnf}}}B^2(t) \\ &+ g\ \text{Cos}\ \phi[(\beta_T)_{\text{hnf}}(T-T_h)(1+(T-T_h)(\beta_T)_{\text{hnf}}) \\ &+ (\beta_C)(C-C_h)(1+(C-C_h)(\beta_C))],\end{aligned} \tag{2}$$

$$\begin{aligned}\frac{\partial T}{\partial t} + v\frac{\partial T}{\partial y} + u\frac{\partial T}{\partial x} &= \alpha_{\text{hnf}}\left[\frac{\partial^2 T}{\partial y^2}\right] \\ &+ \tau\left[D_B\left(\frac{\partial T}{\partial y}\right)\left(\frac{\partial C}{\partial y}\right) - \left(\frac{\partial T}{\partial y}\right)^2\frac{D_T}{T_h}\right] + \sigma_{\text{hnf}}\frac{B^2(t)}{(\rho Cp)_{\text{hnf}}}u,\end{aligned} \tag{3}$$

$$\frac{\partial C}{\partial t} + v\frac{\partial C}{\partial y} + u\frac{\partial C}{\partial x} = D_B\frac{\partial^2 C}{\partial y^2} + \frac{\partial^2 T}{\partial y^2}\frac{D_T}{T_h} - (C-C_\infty)\text{Kr}. \tag{4}$$

The flow constraints at the physical boundaries are

$$\left.\begin{aligned} &v = 0,\ \ u = U_w,\ \ C = C_w,\ \ T = T_w, \quad \text{at } y = 0 \\ &\frac{\partial u}{\partial y} = \frac{\partial T}{\partial y} = \frac{\partial C}{\partial y} = 0,\ \ v = \frac{\partial h}{\partial t}, \quad \text{at } y = h(t) \end{aligned}\right\}, \tag{5}$$

The collection of variables that can undergo transformation is described as follows:

$$\begin{aligned} &u = f'(\eta)\left(\frac{xb}{(1 - t\alpha)}\right),\ \ v = -\left(\left(\frac{b\upsilon}{(1 - t\alpha)}\right)^{1/2} f(\eta)\right), \\ &\eta = y\left(\sqrt{\frac{b}{(1 - t\alpha)\upsilon}}\right). \end{aligned} \tag{6}$$

The resultant equations in dimensionless form are given as

$$\begin{aligned} &f''' + \left(\frac{\mu_f}{\mu_{\text{hnf}}}.\frac{\rho_{\text{hnf}}}{\rho_f}\right)\left[f''f - S\left(f' + \frac{\eta}{2}f''\right) - (f')^2\right] \\ &- M\left(\frac{\sigma_{\text{hnf}}}{\sigma_f}\frac{\mu_f}{\mu_{\text{hnf}}}\right)f' + \left(\frac{\mu_f}{\mu_{\text{hnf}}}\frac{(\rho\beta_T)_{\text{hnf}}}{(\rho\beta_T)_f}\right)[\theta\text{Gr} \\ &+ \theta^2\text{Gr}^*]\,\text{Cos}\,\phi \\ &+ \left(\frac{\rho_{\text{hnf}}}{\rho_f}\frac{\mu_f}{\mu_{\text{hnf}}}\right)[\text{Gc}^*\Phi^2 + \text{Gc}\Phi]\,\text{Cos}\,\phi = 0, \end{aligned} \tag{7}$$

$$\begin{aligned} &\frac{k_{\text{hnf}}}{k_f}\theta'' + \text{Nt}(\theta')^2 + \text{Nb}\theta'\Phi' + \text{Ec}M(f')^2 \\ &+ \text{Pr}\frac{(\rho C_p)_{\text{hnf}}}{(\rho C_p)_f}\left[\theta' f - 2f'\theta - (3\theta + \eta\theta')\frac{S}{2}\right] = 0, \end{aligned} \tag{8}$$

$$\Phi'' + \frac{\text{Nb}}{\text{Nt}}\theta'' + \text{Sc}\left[f\Phi' - 2f'\Phi - \frac{S}{2}(\Phi\eta + 3\Phi)\right] - \Phi\gamma = 0, \tag{9}$$

with related boundary conditions as follows:

$$\begin{aligned} &f(0) = 0,\ \ f'(0) = 1,\ \ f(\beta) = \frac{S\beta}{2},\ \ f''(\beta) = 0, \\ &\theta(0) = 1,\ \ \Phi(0) = 1,\ \ \theta'(\beta) = 0,\ \ \Phi'(\beta) = 0. \end{aligned} \tag{10}$$

The aforementioned physical parameters M, S, Ec, Pr, γ, Sc, Gr, Gr*, G_c, Gc*, N_t, and N_b are mathematically described as

$$\begin{aligned} &M = \frac{\sigma B_0^2}{\rho b},\ \ S = \frac{a}{b},\ \ \text{Ec} = \frac{U_w^2}{c_p(T_w - T_0)},\ \ \text{Pr} = \frac{\upsilon}{\alpha}, \\ &\gamma = \frac{kr}{b},\ \ \text{Gr} = (\beta_T)\frac{g(T_w - T_\infty)}{U_w^2},\ \ \text{Sc} = \frac{\upsilon}{D_B}, \\ &\text{Gr}^* = (\beta_T)^2\frac{g(T_w - T_\infty)^2}{U_w^2},\ \ \text{Gc}^* = (\beta_c)^2\frac{g(C_w - C_\infty)^2}{U_w^2}, \\ &\text{Gc} = (\beta_c)\frac{g(C_w - C_\infty)}{U_w^2},\ \ \text{Nt} = \frac{\tau D_B(T_w - T_\infty)}{\nu T_\infty}, \\ &\text{Nb} = \frac{\tau D_B(C_w - C_\infty)}{\nu}. \end{aligned} \tag{11}$$

The thermophysical properties of nano/hybrid nanofluids are outlined in Table 1, while their corresponding numerical values are presented in Table 2. These tables provide a comprehensive description and quantification of the properties exhibited by the nano/hybrid nanofluids under consideration.

2.1 Interested quantities

The coefficient of skin friction, Nusselt, and Sherwood numbers are the main quantities commonly used in fluid mechanics and heat/mass transfer studies. These quantities are described as follows:

(a) The coefficient of skin friction represents the frictional resistance exerted by a fluid flow on a solid surface. It

Table 2: Computational characteristics of pure fluid and Cu/CuO nanoparticles [33]

	CuO	Cu	Blood
ρ (kg m^{-3})	6500.00	8933.00	1063.00
C_p (J kg^{-1} K^{-1})	533.000	385.000	3594.00
κ (W m^{-1} K^{-1})	17.6500	400.000	0.49200
$\beta \times 10^5$ K^{-1}	1.80000	1.67000	0.18000

Table 1: Thermo-physical characteristics of CuO and CuO + Cu/Blood [32]

	(CuO)/nanofluid	(CuO + Cu/Blood)/hybrid nanofluid
Density	$\rho_{\text{nf}} = \rho_{s1}\varphi_1 + \rho_f(1 - \varphi_1)$	$\rho_{\text{hnf}} = \left\{\left((1 - \varphi_1) + \varphi_1\frac{\rho_{s1}}{\rho_f}\right)(1 - \varphi_2) + \frac{\rho_{s2}}{\rho_f}\varphi_2\right\}\rho_f$
Heat capacity	$(C_p\rho)_{\text{nf}} = (C_p\rho)_f(1 - \varphi_1) + (C_p\rho)_{s1}\varphi_1$	$(\rho C_p)_{\text{hnf}} = (\rho C_p)_f\left\{(1 - \varphi_2)\left((1 - \varphi_1) + \frac{(\rho C_p)_{s1}}{(\rho C_p)_f}\varphi_1\right) + \frac{(\rho C_p)_{s2}}{(\rho C_p)_f}\varphi_2\right\}$
Dynamic viscosity	$\mu_{\text{nf}} = \frac{\mu_f}{(1 - \varphi_1)^{2.5}}$	$\mu_{\text{hnf}} = \frac{\mu_f}{(1 - \varphi_2)^{1/2}(1 - \varphi_1)^{1/2}}$
Thermal conductivity	$\frac{\kappa_{\text{nf}}}{\kappa_f} = \frac{\kappa_{s1} - 2\varphi_1(\kappa_f - \kappa_{s1}) + 2\kappa_f}{\kappa_{s1} + \varphi_1(\kappa_f - \kappa_{s1}) + 2\kappa_f}$	$\frac{\kappa_{\text{hnf}}}{\kappa_{\text{nf}}} = \frac{\kappa_{s2} - 2\varphi_2(\kappa_f - \kappa_{s2}) + 2\kappa_f}{\kappa_{s2} + \varphi_2(\kappa_f - \kappa_{s2}) + 2\kappa_f}$

measures the shear stress between the fluid and the surface and is typically used to assess the flow resistance or drag in various applications.

(b) The Nusselt number is used to analyze the convective heat transfer between the flow of fluid and the surface of the sheet. It helps to measure the transportation of temperature in the flow system.

(c) The Sherwood number is similar to the Nusselt number but is specifically used for mass transfer processes. It quantifies the efficiency of mass transfer, such as the diffusion or convection of a species amid fluid flow and surface. The Sherwood number is used in applications involving mass transfer, such as chemical reactions, absorption processes, and membrane operations.

The mathematical depiction for these quantities is given below:

$$C_{f\infty} = \frac{\tau_w}{\frac{1}{2}\rho U_w^2} = \text{Coefficient of Skin Friction}, \tag{12}$$

$$\text{Nu}_x = \frac{q_w x}{k(T_w - T_0)} = \text{Nusselt Number}, \tag{13}$$

$$\text{Sh}_x = \frac{q_m x}{D_B(C_w - C_0)} = \text{Sherwood Number}. \tag{14}$$

In dimensionless form, these quantities are

$$\text{Re}_\infty^{1/2} C_{f\infty} = -\frac{\mu_{\text{hnf}}}{\mu_f} f''(0) = \text{Coefficient of Skin Friction}, \tag{15}$$

$$\text{Re}_\infty^{1/2} \text{Nu}_x = -\frac{k_{\text{hnf}}}{k_f}\theta'(0) = \text{Nusselt Number}, \tag{16}$$

$$\text{Re}_\infty^{1/2} \text{Sh}_x = -\phi'(0) = \text{Sherwood Number}. \tag{17}$$

2.2 Entropy analysis

It is mathematically defined as

$$\begin{aligned} S'''_{\text{gen}} = {} & \frac{k_{\text{hnf}}}{T_h^2}\left[\left(\frac{\partial T}{\partial y}\right)^2\right] + \frac{\mu_{\text{hnf}}}{T_h}\left(\frac{\partial u}{\partial y}\right)^2 + \frac{\sigma_{\text{hnf}} B_0^2 u^2}{T_h} \\ & + \frac{g}{T_h}[(\beta_T)_{\text{hnf}}(T - T_h)[1 + (\beta_T)_{\text{hnf}}(T - T_h)]]\,\text{Cos}\,\theta \\ & + \frac{g}{T_h}[(\beta_C)(C - C_h)[1 + (\beta_C)(C - C_h)]]\text{Cos}\,\theta \\ & + \frac{\text{RD}}{C_h}\left(\frac{\partial C}{\partial y}\right)^2 + \frac{\text{RD}}{T_h}\left(\frac{\partial T}{\partial y}\frac{\partial C}{\partial y} + \frac{\partial C}{\partial x}\frac{\partial T}{\partial x}\right), \end{aligned} \tag{18}$$

$$\begin{aligned} S_G = {} & \alpha_1 \frac{k_{\text{hnf}}}{k_f}(\theta')^2 + \text{Br}\frac{\mu_{\text{hnf}}}{\mu_f}(f'')^2 + Mf' \\ & + \frac{\beta_{T\ \text{hnf}}}{\beta_{T\ f}}(\text{Gr}(\theta)^2 + \text{Gr}^*(\theta)^2 + \text{Gc}\Phi + \text{Gc}^*(\Phi)^2) \\ & + L\left(\theta'\Phi' + \frac{\alpha_2}{\alpha_1}(\Phi')^2\right). \end{aligned} \tag{19}$$

2.3 Bejan number

It is described as

$$\text{Be} = \frac{\text{Irreversibility due to heat and mas transfer}}{\text{Total irreversilbility}}, \tag{20}$$

$$\text{Be} = \frac{\alpha_1 \frac{k_{\text{hnf}}}{k_f}(\theta')^2 + L\left(\theta'\Phi' + \frac{\alpha_2}{\alpha_1}(\Phi')^2\right)}{\begin{pmatrix} \alpha_1 \frac{k_{\text{hnf}}}{k_f}(\theta')^2 + \text{Br}\frac{\mu_{\text{hnf}}}{\mu_f}(f'')^2 + Mf' \\ + L\left(\theta'\Phi' + \frac{\alpha_2}{\alpha_1}(\Phi')^2\right) \\ \frac{\beta_{T\ \text{hnf}}}{\beta_{T\ f}}(\text{Gr}(\theta)^2 + \text{Gr}^*(\theta)^2 + \text{Gc}\Phi + \text{Gc}^*(\Phi)^2) \end{pmatrix}}, \tag{21}$$

with

$$\begin{gathered} S_G = \frac{S_{\text{gen}} \upsilon T_h}{k_f \Delta T}, \quad \Delta T = T_w - T_h, \quad \alpha_1 = \frac{\Delta T}{T_h}, \quad \alpha_2 = \frac{\Delta C}{C_h}, \\ \Delta C = C_w - C_h, \quad L = \frac{\text{RD}\Delta C}{k_f}. \end{gathered} \tag{22}$$

3 Solution method

The solution of Eqs. (7)–(9) subject to Eq. (10) has been evaluated by using HAM [34,35]. The presented approach is a semi-analytical method that exhibits rapid convergence, making it suitable for solving nonlinear differential equations. To apply this approach, some starting values are necessary. For the current problem, these starting values are provided as follows:

$$f_0(\eta) = S + \eta, \quad \phi_0(\eta) = 1, \quad \theta_0(\eta) = 1, \tag{23}$$

with

$$\widehat{L_f} = f''', \quad \widehat{L_\phi} = \phi'', \quad \widehat{L_\theta} = \theta''. \tag{24}$$

Such that

$$\widehat{L_f}(a_3 + \eta a_2 + \eta^2 a_1) = 0, \quad \widehat{L_\theta}(a_5 + \eta a_4) = 0, \quad \widehat{L_\phi}(a_7 + \eta a_6) = 0, \tag{25}$$

where $a_i (i = 1 \to 7)$ are fixed values.

4 Results and discussion

This work investigates thin film flow with the effects of a magnetic field in association with Cu and CuO nanoparticles past an inclined plate. The thickness of the film is taken as a variable to sustain the uniformity of the thin film for sliding on the surface, while the dragging terminology is taken as nonlinear for the flow of film down the plate. To optimize the production of entropy and to reduce the fluid's friction, the second law of thermodynamics is employed. Additionally, the current model supplements by incorporating the collective role of mass and heat transportation. Some emerging factors have been collected in the modeling of the problem; the influence of these factors will be deliberated in the following paragraphs.

4.1 Velocity distribution

The variations in velocity characteristics in response of different values of emerging factors are shown in Figure 2(a)–(i). Figure 2(a) illustrates the impact of magnetic forces on fluid motion. As the Lorentz force increases for growth in M, it generates a resistive force in the fluid against the velocity of nanoparticles, resulting in heightened resistance experienced by the fluid particles. During this process, the fluid velocity drops as M escalates. The impression of thickness factor β upon fluid motion is depicted in Figure 2(b). The observed trend in this figure reveals that as thickness of fluid film upsurges, the fluid particles move more slowly along the inclined plate, indicating a reduction in their downward motion. Indeed, as the values of β increase, greater cohesion is observed among the fluid particles. This increased cohesion results in reduced fluid motion. Figure 2(c) and (d) show the influences of thermal and nonlinear thermal Grashof numbers (Gr, Gr^*) upon fluid motion. In these figures, an augmenting behavior has been observed in fluid flow characteristics for intensification in the values of (Gr, Gr^*). Similarly, for growth in mass Grashof and nonlinear mass Grashof numbers (G_C, G_C^*), there is an expansion in the velocity panels as shown in Figure 2(e) and (f). Physically, this can be understood as for upsurge in Grashof number the viscous force weakens due to which the liquid particles observed minimum constraints in flow direction. This phenomenon is more remarkable in case of nonlinear factors Gr^* as depicted in Figure 2(d) and for Gc^* as shown in Figure 2(f). The impact of ϕ_1, ϕ_2(volume fractions) on fluid flow characteristics is observed in Figure 2(g). It is noticed that with growth in ϕ_1, ϕ_2 there is retardation in fluid motion. Actually, for surge in ϕ_1, ϕ_2, the fluid behaves in more dense manners due to which fluid's nanoparticles experience more resistance in the direction of their motion. In this process, the fluid motion of nanoparticles upon the inclined sheet becomes less as illustrated in Figure 2(g). The influence of λ over fluid motion is shown in Figure 2(h) where a deteriorating behavior of $f'(\eta)$ has been noticed in response of growth in the values of λ. Since λ describes the connection between relaxation and retardation times, so with upsurge in λ there is more resistive force to fluid particles transportation. In this process, the fluid flow characteristics declines as shown in Figure 2(h). The impression of unsteadiness factor S over fluid's motion is illustrated in Figure 2(i) with retarding behavior in the flow characteristics. Since, with growth in S, more friction is created in the line of fluid motion; hence with growth in S, the fluid motion declines as depicted in Figure 2(i).

4.2 Thermal distribution

The effect of numerous factors on thermal distribution is depicted in Figure 3(a)–(f). In Figure 3(a), it has been revealed that the growing values of magnetic factor M support the thermal transportation. Actually, for upsurge in M, there is more resistive force among fluid particles in the opposite direction of fluid motion. Due to these resistive forces, the skin friction augments and ultimately thermal energy enlarges that supports the growth in temperature distribution. The influences of volume fraction ϕ_1, ϕ_2 upon energy distribution are illustrated in Figure 3(b) with an enlarging behavior as perceived in heat profiles. Actually, with growth in ϕ_1, ϕ_2 the dense behavior of fluid augments for which additional constraints is practiced by the fluid particles. In this phenomenon, the fluid motion has declined while the energy distribution has augmented as explained in Figure 3(b). Growth in Eckert number Ec also supports the thermal distribution as shown in Figure 3(c). The thermal dissipative properties are primarily governed by Ec at the free surface, resulting in the efficient gathering of energy among the fluid particles near boundary on the inclined plate. So the thermal distribution is escalated with higher values of Ec. Figure 3(d) shows the expansion in strength of thermal layer at boarder-line with expansion in S. This states that in steady-state conditions, nanoparticles cool at a faster rate, whereas in time-

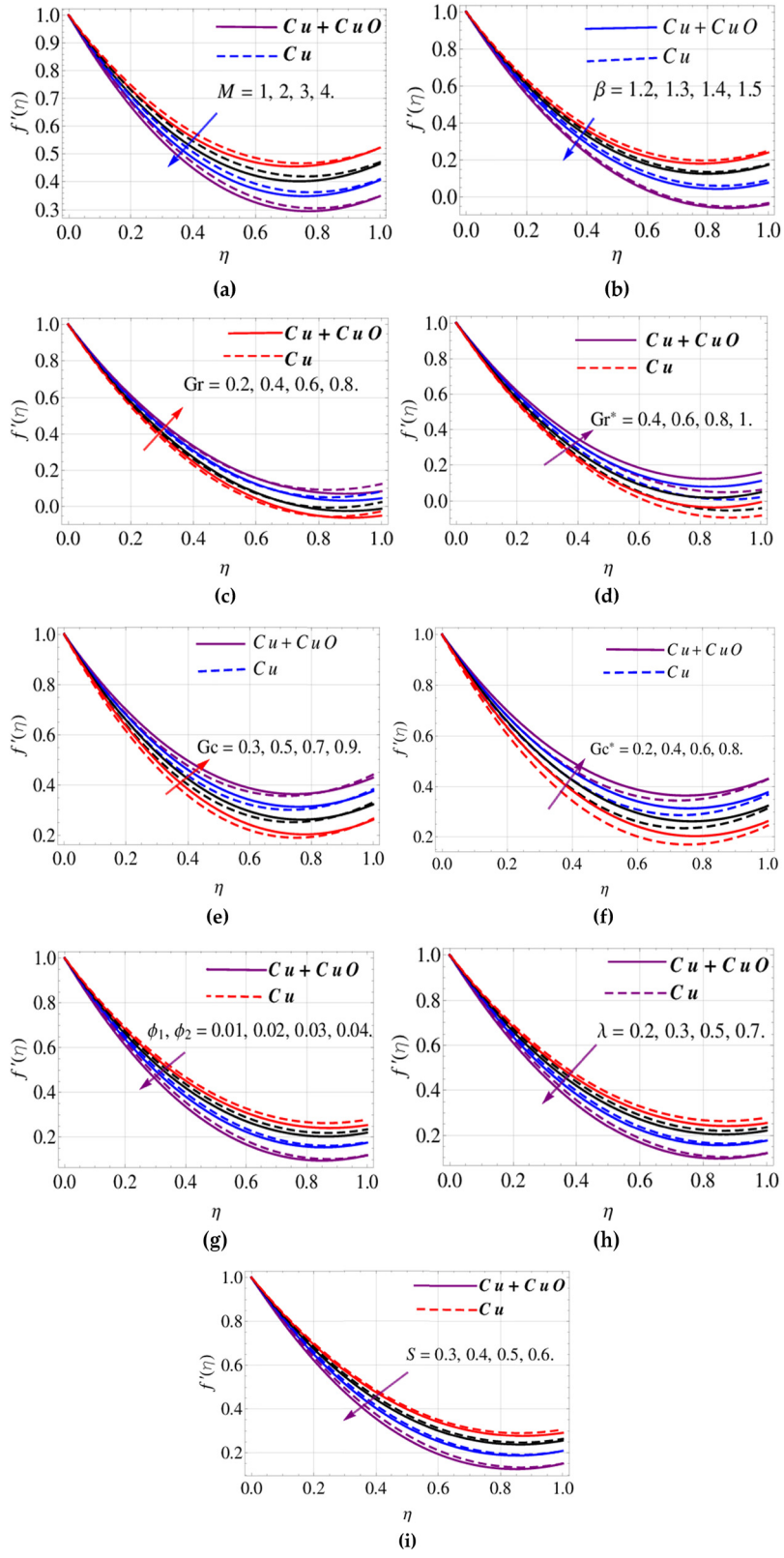

Figure 2: (a–i) Impact of various emerging factors on velocity distribution.

dependent scenarios, a longer duration is needed for this phenomenon to occur. The influence of Brownian motion factor Nb on thermal panels is shown in Figure 3(e). Clearly with escalation in Nb, the zigzag motion among the nanoparticles escalates as a consequence the kinetic energy is converted to thermal energy. As a result, maximum thermal diffusion occurs that augment thermal distribution as shown in Figure 3(e). The effect of Nt on temperature distribution is depicted in Figure 3(f) with a growing manner in thermal profiles. Since Nt is described mathematically as $\mathrm{Nt} = \tau D_B(T_w - T_\infty)/\nu T_\infty$, so growth in Nt supports the temperature gradient at free stream of the inclined plate, for which more heat is shifted from high to low temperature zone. In this process, thermal diffusion is at its peak; hence, thermal distribution upsurges with escalated values of Nt as shown in Figure 3(f).

4.3 Concentration distribution

The impact of chemical reaction factor γ on diffusions of mass is presented in Figure 4(a). With an upsurge in γ, the diffusions of mass augments and results in the growth of concentration boundary. Through this process, the concentration distribution augment is shown in Figure 4(a). The influence of Schmidt number Sc is given in Figure 4(b). It is noticed from this figure that concentration distribution

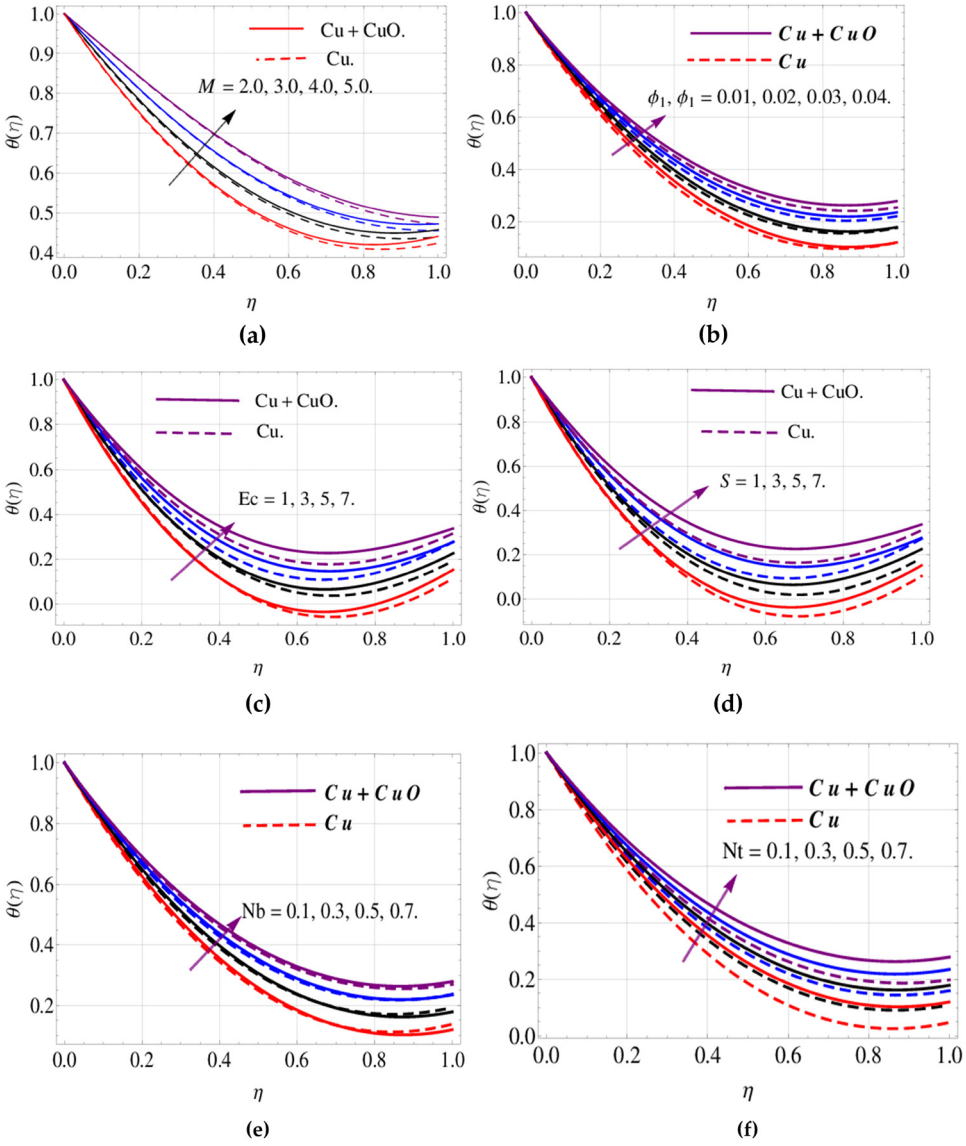

Figure 3: (a–f) Impact of different emerging factors upon thermal distribution.

$\Phi(\eta)$ declines with growth in Sc. Actually, Sc is in inverse relation to diffusion of mass, so augmentation in Sc means reduction in diffusion of mass that results in the drop of concentration distribution $\Phi(\eta)$. Figure 4(c) depicts that with upsurge in unsteadiness factor S there is a decline in concentration profiles $\Phi(\eta)$. This can be interpreted as, for upsurge in S more time is required for mass to be diffused as compared to steady case. Hence, with growth in S, there is a decline in concentration distribution $\Phi(\eta)$. Figure 4(d) and (e) show the impacts of N_b and N_t on concentration distribution $\Phi(\eta)$. Upsurge in N_b reduces the profiles of $\Phi(\eta)$, whereas adverse effects have been noticed for growth in N_t against the profiles of $\Phi(\eta)$. For growth in N_b, there is a decline in nanoparticles volume fraction at free surface that retards the concentration distribution as depicted in Figure 4(d). Conversely, for progression in N_t, the diffusion of mass upsurge that results in the growth of concentration distribution $\Phi(\eta)$ as illustrated in Figure 4(e).

4.4 Bejan number and generation of entropy rate

Variations in irreversibility generation and Bejan number in the reaction of changes in various substantial factors are

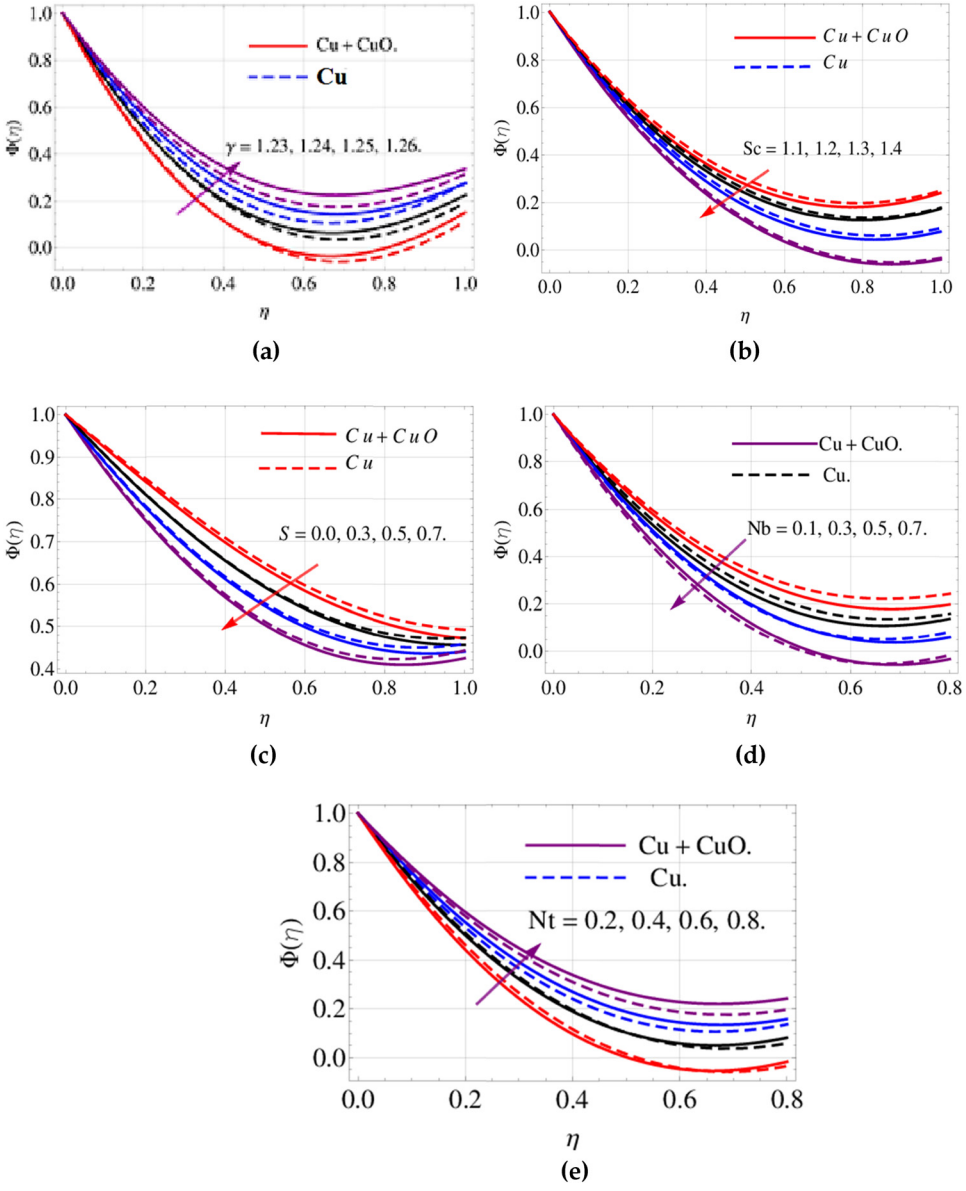

Figure 4: (a–e) Impact of various factors on concentration profiles.

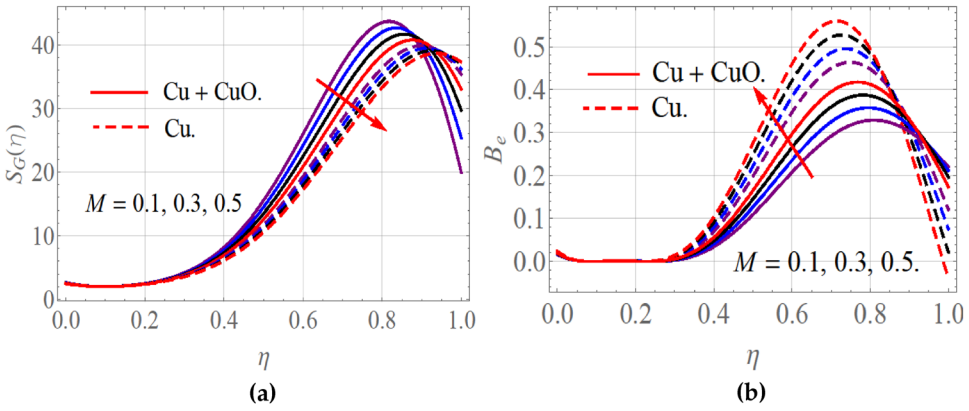

Figure 5: (a, b) Bejan number and entropy *vs* variations in M.

discussed in Figures 5 and 6. The influence of M on entropy and Bejan number is shown in Figure 5(a) and (b). It is obvious that with higher M nanoparticles experience more restrain during motion that resulting in more disturbance in the flow pattern of fluid and producing more entropy, as illustrated in Figure 5(a). In this physical phenomenon, the Bejan number enhances as shown in Figure 5(b).

Figure 6(a) and (b) present the influence of Br on entropy and Bejan number. It has been noticed that for growth in Br, entropy rate has augmented. Actually, Br let out the thermal flow through the conductance of molecules with an association of heat transportation to the viscous thermal flow of fluid particles. Moreover, for augmentation in Br, the thermal conductance of nanoparticles retards continuously that results in augmentation of irreversibility generation rate as shown in Figure 6(a). In this physical phenomenon, it has been observed that the Bejan number experiences a deceleration, as illustrated in Figure 6(b).

4.5 Discussion of tables

The thermo-physical properties of CuO and CuO + Cu/Blood is presented in Table 1 with their numerical values in Table 2. From Table 3, it is noticed that augmentation in thermal as well as nonlinear thermal Grashof numbers has upsurge the fluid motion while it is declined for higher magnetic factor, volumetric fraction, thickness, and unsteadiness factors. Therefore, skin friction has upsurge for progression in magnetic factor, volumetric fraction, thickness, and unsteadiness factors and has declined with growth in thermal as well as nonlinear thermal Grashof numbers. In Table 4, it is revealed that Nusselt number has augmented for growth in volume fraction, Ecker number, magnetic factor, unsteadiness effects, Brownian motion number, and thermophoresis factor. Table 5 depicts percentage variation in Nusselt number for Cu as well as Cu + CuO nanoparticles. It has been observed in this table that when there is a variation in volume fraction from 0.01 to 0.02, Nusselt number boots

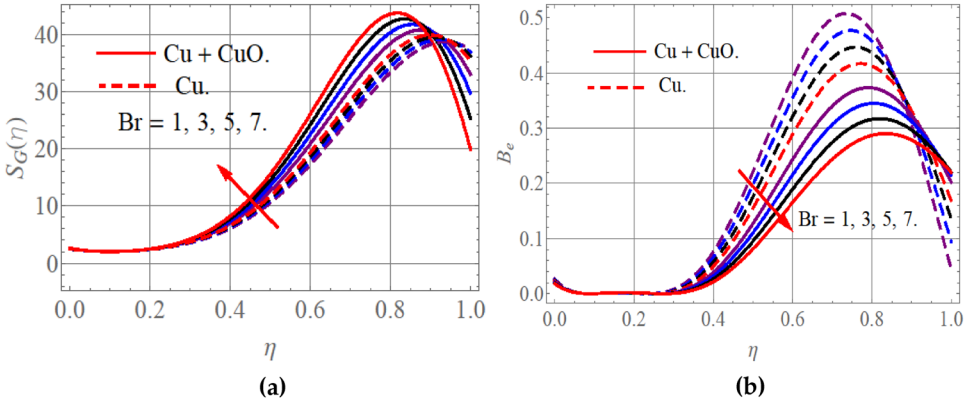

Figure 6: (a, b) Entropy and Bejan number *vs* variations in Brinkman number Br.

Table 3: Skin friction ($\mathrm{Re}_r^{1/2}C_{fr} = (\mu_{\mathrm{hnf}}/\mu_f)f''(0)$) *vs* variations in various factors

Gr	Gr*	ϕ_1, ϕ_2	S	M	Gc	Gc*	Cu $(\mu_{\mathrm{nf}}/\mu_f)f''(0)$	Cu + CuO $(\mu_{\mathrm{hnf}}/\mu_f)f''(0)$
0.1	0.1	0.01	0.1	0.5	0.1	0.1	0.63532180	0.636976420
0.2							0.63421070	0.632057420
0.3							0.63310060	0.631424113
	0.2						0.63376542	0.632334620
	0.3						0.63201343	0.631307600
		0.02					0.64876530	0.649965421
		0.03					0.65210990	0.655321090
			0.3				0.64321870	0.653201700
			0.5				0.65372100	0.654865327
				0.7			0.64076523	0.645879650
				0.9			0.64387652	0.646487990
					0.2		0.63201564	0.631654231
					0.3		0.63021032	0.628764532
						0.2	0.63003421	0.627643210
						0.3	0.62978650	0.627456321

Table 4: Nusselt number ($\mathrm{Re}_r^{1/2}\mathrm{Nu}_r = -k_{\mathrm{hnf}}/k_f\theta'(0)$) *vs* variations in various factors

Nt	S	M	Nb	Ec	Cu $(-k_{\mathrm{nf}}/k_f\theta'(0))$	Cu + CuO $(-k_{\mathrm{hnf}}/k_f\theta'(0))$
6.2	1.3	1.0	0.1	1	4.2654318	4.276743210
6.4					4.2689043	4.277453210
6.6					4.2896534	4.298703210
	1.3				4.2965329	4.310965334
	1.6				4.30721545	4.358703212
		1.5			4.3477930	4.380987400
		2			4.3567440	4.399767000
			0.3		4.3202100	4.348743000
			0.5		4.3454320	4.356798540
				2	4.4578242	4.460241780
				3	4.5321098	4.567320210

from 2.990 to 4.327% for Cu-nanoparticles whereas in case of Cu + CuO-nanoparticles, this jump in Nusselt number is from 4.3207 to 6.6983% for the same range of nanoparticles concentration. This reveals the dominancy of hybrid nanofluid over normal nanofluid. Sherwood number has an augmentation for higher values of thermophoresis factor while it is degenerated for higher values of Brownian motion and Schmidt factor as shown in Table 6. To validate the current work, its results are compared with the established findings of Li *et al.* [36] and Ali *et al.* [37] in Table 7. It is evident from this table that a strong agreement exists among all the results, confirming the validity of the current work.

Table 6: Sherwood number against variations in various factors

Sc	Nb	S	Nt	$-(D_{\mathrm{nf}}/D_f)\Phi'(0)$ Cu	$-(D_{\mathrm{hnf}}/D_f)\Phi'(0)$ Cu + CuO
1.5	0.1	0.1	0.1	5.3202511	5.32187542
2.5				5.3002190	3.35867100
3.5				5.2768590	3.30561900
	0.3			5.4532800	3.47316900
	0.5			5.5021800	3.53543500
		0.3		5.3028710	3.58983500
		0.5		5.2654230	4.96657400
			0.3	5.5289000	4.71948700
			0.5	5.6432100	4.52376700

Table 5: Percentage variation in Nusselt number with growth in nanoparticles (by using the relation % Increase = $\frac{\text{With Nanoparticles}}{\text{Without Nanoparticles}} \times 100$ = Result, Result − 100 = % enhancment)

ϕ_1, ϕ_2	$-k_{\mathrm{nf}}/k_f\theta'(0)$ for Cu-nanoparticles	$-k_{\mathrm{hnf}}/k_f\theta'(0)$ for Cu + CuO-nanoparticles
0.00	4.3124360	4.3124360
0.01	4.4415471 (2.99000 Increase)	4.4987647 (4.32070 Increase)
0.02	4.4467865 (3.1150% Increase)	4.5403245 (5.2840% Increase)
0.03	4.499032 (4.3270% Increase)	4.6012997 (6.6983% Increase)

Table 7: Results validation with the published studies

Li *et al.* [36] results		Ali *et al.* [37] results		Present results	
β	$f''(0)$	β	$f''(0)$	β	$f''(0)$
4.981455	−1.134	4.981468	−1.1340957	4.981448	−1.1340893
3.131924	−1.195	3.131711	−1.1951252	3.131752	−1.1951289
2.152366	−1.246	2.152021	−1.2458064	2.1520894	−1.24580642
1.543592	−1.278	1.543615	−1.2777693	1.5436782	−1.27776786
1.127783	−1.279	1.127779	−1.2791718	1.1277829	−1.27917493
0.821033	−1.234	0.821031	−1.2335453	0.8213592	−1.23354780
0.576173	−1.115	0.576174	−1.1149368	0.5763576	−1.11493563
0.356389	−0.8674	0.356387	−0.8674104	0.3563981	−0.86741284

5 Conclusions

An endeavor has been made in this study to investigate thin film flow with the effects of a magnetic field in association with Cu and CuO nanoparticles past an inclined plate. To optimize the production of entropy and to reduce the fluid's friction, the second law of thermodynamics is employed. Additionally, the current model supplements by incorporating the combined role of mass and heat transportation. After implementing similarity variables, the leading equations have been converted to dimensionless form and subsequently solved using HAM. After a comprehensive examination of the work, the following observations have been made:

- Fluid motion slows down with increasing values of the thickness factor, magnetic effects, nanoparticle volume fraction, and unsteadiness parameter. In contrast, it intensifies with higher mass and thermal Grashof numbers in both linear and nonlinear scenarios.
- Thermal profiles rise with increases in magnetic parameter, Eckert number, nanoparticle concentration, unsteadiness, thermophoresis, and Brownian motion factors. Physically, these factors enhance thermal energy generation, reduce heat dissipation, and facilitate nanoparticle-induced thermal transport, causing more noticeable temperature gradients.
- Concentration profiles decline with higher Brownian motion, unsteadiness factors, and Schmidt number, while a surge in chemically reactive factors and thermophoresis parameters leads to an upward trend regarding the concentration profiles.
- Entropy generation is enhanced by magnetic effects and reduced by a higher Brinkman number.
- The Bejan number decreases with increasing Brinkman number but increases under stronger magnetic field effects.
- For nanoparticle volume fractions ranging from 0.01 to 0.03, the Nusselt number shows significant improvement, particularly for hybrid nanoparticles, where it increases from 4.3207 to 6.6983%, demonstrating their superiority over traditional nanoparticles.
- Finally, the results of this study show strong agreement with established findings, confirming the accuracy and reliability of the current work.

Acknowledgments: The authors thank Princess Nourah bint Abdulrahman University Researchers Supporting Project number (PNURSP2025R371) and Princess Nourah bint Abdulrahman University, Riyadh, Saudi Arabia.

Funding information: This work was supported by the Princess Nourah bint Abdulrahman University Researchers Supporting Project number (PNURSP2025R371) and Princess Nourah bint Abdulrahman University, Riyadh, Saudi Arabia.

Author contributions: Dr. Arshad Khan and Dr. Mashael A. Aljohani have modeled the problem in mathematical form. Dr. Zehba Raizah and Dr. Khadijah M. Abualnaja have solved the modeled problem through Mathematica software. Dr. Arshad Khan and Dr. Emad E. Mahmoud sketched the graph and discussed the impacts of emerging parameters on various flow profiles and quantities of engineering interest in tabular form. Dr. Humaira Yasmin, Dr. Zehba Raizah, and Dr. Khadijah M. Abualnaja wrote the draft of the manuscript. Dr. Wafa F. Alfwzan has contributed during the revision process. All authors have accepted responsibility for the entire content of this manuscript and approved its submission.

Conflict of interest: The authors state no conflict of interest.

Data availability statement: The datasets generated and/or analysed during the current study are available from the corresponding author on reasonable request.

References

[1] Wang CY. Thin film flowing down a curved surface. Z Für Angew Math Und Phys ZAMP. 1984;35(4):532–44.

[2] Qasim M, Khan ZH, Lopez RJ, Khan WA. Heat and mass transfer in nanofluid thin film over an unsteady stretching sheet using Buongiorno's model. Eur Phys J Plus. 2016;131(1):1–11.

[3] Sun TC, Uddin I, Raja MAZ, Shoaib M, Ullah I, Jamshed W, et al. Numerical investigation of thin-film flow over a rotating disk subject to the heat source and nonlinear radiation: Lobatto IIIA approach. Waves Random Complex Media. 2025;35(1):888–902.

[4] Kapitza PL, Kapitza SP, Kapitza PL, Kapitza SP. Wave flow of thin layers of viscous liquids. Part III. Experimental research of a wave flow regime. ZhETF. 1949;19:105–20.

[5] Dholey S. Instabilities of a thin viscoelastic liquid film flowing down an inclined plane in the presence of a uniform electromagnetic field. Rheol Acta. 2017;56(4):325–40.

[6] Crane LJ. Flow past a stretching plate. Z Für Angew Math Und Phys ZAMP. 1970;21(4):645–7.

[7] Sudarmozhi K, Iranian D, Alessa N. Investigation of melting heat effect on fluid flow with brownian motion/thermophoresis effects in the occurrence of energy on a stretching sheet. Alex Eng J. 2024;94:366–76.

[8] Roşca NC, Pop I. Unsteady boundary layer flow over a permeable curved stretching/shrinking surface. Eur J Mech, B/Fluids. 2015;51:61–7.

[9] Abbas Z, Naveed M, Sajid M. Hydromagnetic slip flow of nanofluid over a curved stretching surface with heat generation and thermal radiation. J Mol Liq. 2016;215:756–62.

[10] Imtiaz M, Hayat T, Alsaedi A, Hobiny A. Homogeneous-heterogeneous reactions in MHD flow due to an unsteady curved stretching surface. J Mol Liq. 2016;221:245–53.

[11] Sanni KM, Asghar S, Jalil M, Okechi NF. Flow of viscous fluid along a nonlinearly stretching curved surface. Results Phys. 2017;7:1–4.

[12] Hayat T, Aziz A, Muhammad T, Alsaedi A. Numerical study for nanofluid flow due to a nonlinear curved stretching surface with convective heat and mass conditions. Results Phys. 2017;7:3107–15.

[13] Okechi NF, Jalil M, Asghar S. Flow of viscous fluid along an exponentially stretching curved surface. Results Phys. 2017;7:2851–4.

[14] Yasmin H, Shahab S, Lone SA, Raizah Z, Saeed A. Convective flow of a magnetohydrodynamic second-grade fluid past a stretching surface with Cattaneo–Christov heat and mass flux model. Open Phys. 2024;22(1):20230204.

[15] Anwar MS, Irfan M, Muhammad T. Non-Newtonian fluid flow over a stretching sheet in a porous medium with variable thermal conductivity under magnetohydrodynamics influence. ZAMM-J Appl Math Mech/Z für Angew Math und Mechanik. 2024;104(12):e202301048.

[16] Lone SA, Khan A, Raiza Z, Alrabaiah H, Shahab S, Saeed A, et al. A semi-analytical solution of the magnetohydrodynamic blood-based ternary hybrid nanofluid flow over a convectively heated bidirectional stretching surface under velocity slip conditions. AIP Adv. 2024;14(4):1–13.

[17] Hobiny AD, Abbas IA. Nonlinear analysis of dual-phase lag bio-heat model in living tissues induced by laser irradiation. J Therm Stresses. 2020;43(4):503–11.

[18] Ali A, Khan Z, Sun M, Muhammad T, Alharbi KAM. Numerical investigation of heat and mass transfer in micropolar nanofluid flows over an inclined surface with stochastic numerical approach. Eur Phys J Plus. 2024;139(10):1–25.

[19] Khader MM, Ahmad H, Adel M, Megahed AM. Numerical analysis of the MHD Williamson nanofluid flow over a nonlinear stretching sheet through a Darcy porous medium: Modeling and simulation. Open Phys. 2024;22(1):20240016.

[20] Alkaoud A, Khader MM, Eid A, Megahed AM. Numerical simulation for the slip impacts on the radiative nanofluid flow over a stretched surface with nonuniform heat generation and viscous dissipation. Open Phys. 2024;22(1):20240028.

[21] Dinarvand S, Nademi Rostami M, Dinarvand R, Pop I. Improvement of drug delivery micro-circulatory system with a novel pattern of CuO-Cu/blood hybrid nanofluid flow towards a porous stretching sheet. Int J Numer Methods Heat Fluid Flow. 2019;29(11):4408–29.

[22] Shojaie Chahregh H, Dinarvand S. TiO_2-Ag/blood hybrid nanofluid flow through an artery with applications of drug delivery and blood circulation in the respiratory system. Int J Numer Methods Heat Fluid Flow. 2020;30(11):4775–96.

[23] Chamkha AJ, Rashad AM, Al-Mudhaf HF. Heat and mass transfer from truncated cones with variable wall temperature and concentration in the presence of chemical reaction effects. Int J Numer Methods Heat Fluid Flow. 2012;22(3):1120–8.

[24] Khan A, Saeed A, Tassaddiq A, Gul T, Kumam P, Ali I, et al. Bio-convective and chemically reactive hybrid nanofluid flow upon a thin stirring needle with viscous dissipation. Sci Rep. 2021;11(1):8066.

[25] Gul T, Akbar R, Zaheer Z, Amiri IS. The impact of the Marangoni convection and magnetic field versus blood-based carbon nanotube nanofluids. Proc Inst Mech Eng, Part N: J Nanomater, Nanoeng Nanosyst. 2020;234:1–2.

[26] Kamis NI, Basir MFM, Shafie S, Khairuddin TKA, Jiann LY. Suction effect on an unsteady Casson hybrid nanofluid film past a stretching sheet with heat transfer analysis. IOP Conf Ser: Mater Sci Eng. 2021;1078(1):012019.

[27] Hobiny A, Abbas I. Thermal response of cylindrical tissue induced by laser irradiation with experimental study. Int J Numer Methods Heat Fluid Flow. 2020;30(8):4013–23.

[28] Marin M, Hobiny A, Abbas I. Finite element analysis of nonlinear bioheat model in skin tissue due to external thermal sources. Mathematics. 2021;9(13):1459.

[29] Eid MR, Mabood F, Mahny KL. On 3D Prandtl nanofluid flow with higher-order chemical reaction. Proc Inst Mech Eng, Part C: J Mech Eng Sci. 2021;235(19):3962–74.

[30] Dhlamini M, Kameswaran PK, Sibanda P, Motsa S, Mondal H. Activation energy and binary chemical reaction effects in mixed convective nanofluid flow with convective boundary conditions. J Comput Des Eng. 2019;6(2):149–58.

[31] Saeed T, Abbas I. Finite element analyses of nonlinear DPL bioheat model in spherical tissues using experimental data. Mech Based Des Struct Mach. 2022;50(4):1287–97.

[32] Khan A, Hassan B, Ashraf EE, Shah SYA. Thermally dissipative micropolar hybrid nanofluid flow over a spinning needle influenced by Hall current and gyrotactic microorganisms. Heat Transf. 2022;51(1):1170–92.

[33] Jawad M, Khan A, Shah SAA. Examination of couple stress hybrid nanoparticles (CuO-Cu/Blood) as a targeted drug carrier with magnetic effects through porous sheet. Braz J Phys. 2021;51(4):1096–107.

[34] Liao SJ. Explicit totally analytic approximate solution for blasius viscous flow problems. Int J Non-Linear Mech. 1999;34:759–78.
[35] Liao SJ. An optimal homotopyanalysis approach for strongly nonlinear differential equations. Commun Nonlinear Sci Numer Simul. 2010;15:2003–16.
[36] Li J, Liu L, Zheng L, Bin-Mohsin B. Unsteady MHD flow and radiation heat transfer of nanofluid in a finite thin film with heat generation and thermophoresis. J Taiwan Inst Chem Eng. 2016;67:226–34.
[37] Ali R, Shahzad A, us Saher K, Elahi Z, Abbas T. The thin film flow of Al_2O_3 nanofluid particle over an unsteady stretching surface. Case Stud Therm Eng. 2022;29:101695.